Inorg. Chem. **2008**, *47*, 9857−9869

Inorganic Chemistry
Article

Probing the Solvent Dependent Photophysics of *fac*-[Re(CO)$_3$(dppz-X$_2$)Cl] (dppz-X$_2$ = 11,12-X$_2$-dipyrido[3,2-a:2′,3′-c]phenazine); X = CH$_3$, H, F, Cl, CF$_3$)

Marina K. Kuimova,[†,‡] Wassim Z. Alsindi,[†] Alexander J. Blake,[†] E. Stephen Davies,[†] Daniele J. Lampus,[†] Pavel Matousek,[§] Jonathan McMaster,[†] Anthony W. Parker,[§] Michael Towrie,[§] Xue-Zhong Sun,[†] Claire Wilson,[†] and Michael W. George*[,†]

School of Chemistry, University of Nottingham, University Park, Nottingham, NG7 2RD, U.K., and Central Laser Facility, Science and Technology Facilities Council, Rutherford Appleton Laboratory, Chilton, Didcot, Oxfordshire

Received April 26, 2008

The results of electrochemical measurements, density-functional theory calculations, emission and time -resolved IR (TRIR) spectroscopic studies for *fac*-[ReCl(CO)$_3$(dppz-X$_2$)], (dppz = dipyrido[3,2-a:2′,3′-c]phenazine; X = CH$_3$, H, F, Cl, CF$_3$) are reported. For all complexes the calculations show that the lowest unoccupied molecular orbital (LUMO) is a phenazine based orbital localized on the dppz ligand. We observe that three different excited states, IL $\pi\pi^*$, metal-to-ligand charge-transfer (MLCT) (phen), and MLCT (phz), are formed depending upon the substituent on the dppz ligand and on the nature of the solvent. This means that both the energy and the nature of the photophysically active state(s) can be tuned by both chemical modification of dppz ligand and solvent properties. The excited-state dynamics in these systems is directly related to the mechanism of the *"light switch effect"*, and ps-TRIR has allowed a deeper insight into this mechanism by being able to directly monitor the change in the population of the higher lying emissive phen-type ^{3}MLCT and IL $\pi\pi^*$ states and the dark ^{3}MLCT (phz) state depending on the different environmental factors.

Introduction

The photophysics of transition metal complexes containing the dppz ligand (dppz = dipyrido[3,2-a:2′,3′-c]phenazine) is the subject of intense research efforts.[1] The dppz ligand may be considered as a fusion of phenanthroline (phen) and phenazine (phz) units and possesses two sets of acceptor orbitals that are close in energy.[2] [M(α-*diimine*)$_2$(dppz)]$^{2+}$ (M = Ru^{II}, Os^{II}; α-*diimine* = bpy, phen) have been investigated extensively since they can serve as luminescent probes of DNA and DNA-mediated electron transfer.[1,3] These complexes can exhibit *"the light switch effect"*, that is, they are luminescent when intercalated into the DNA double helix and in organic solvents but nonemissive in pure aqueous solution in the absence of DNA.[4] The emission can be switched on when these complexes are intercalated into the DNA double helix. This behavior has been attributed to the interplay between two closely lying ^{3}MLCT (MLCT, metal-to-ligand charge-transfer; IL, intraligand) excited states, originating from two acceptor orbitals of different nature: ^{3}MLCT (phen) is emissive and ^{3}MLCT (phz) is dark. It has been suggested that for [Ru(phen)$_2$(dppz)]$^{2+}$ the emission

* To whom correspondence should be addressed. E-mail: mike.george@nottingham.ac.uk.
† University of Nottingham.
‡ Present address: Chemistry Department, Imperial College London, Exhibition Road, SW7 2AZ, U.K.
§ Rutherford Appleton Laboratory.

(1) (a) Erkkila, K. E.; Odom, D. T.; Barton, J. K. *Chem. Rev.* **1999**, *99*, 2777. (b) Metcalfe, C.; Thomas, J. A. *Chem. Soc. Rev.* **2003**, *32*, 215.
(2) (a) Fees, J.; Kaim, W.; Moscherosch, M.; Matheis, W.; Klima, J.; Krejcik, M.; Zalis, S. *Inorg. Chem.* **1993**, *32*, 166. (b) Fees, J.; Ketterle, M.; Klein, A.; Fiedler, J.; Kaim, W. *J. Chem. Soc., Dalton Trans.* **1999**, 2595.
(3) (a) Jenkins, Y.; Friedman, A. E.; Turro, N. J.; Barton, J. K. *Biochemistry* **1992**, *31*, 10809. (b) Friedman, A. E.; Chambron, J. C.; Sauvage, J. P.; Turro, N. J.; Barton, J. K. *J. Am. Chem. Soc.* **1990**, *112*, 4960. (c) Hiort, C.; Lincoln, P.; Norden, B. *J. Am. Chem. Soc.* **1993**, *115*, 3448.
(4) (a) Hiort, C.; Lincoln, P.; Norden, B. *J. Am. Chem. Soc.* **1993**, *115*, 3448. (b) Friedman, A. E.; Kumar, C. V.; Turro, N. J.; Barton, J. K. *Nucleic Acids Res.* **1991**, *19*, 2595. (c) Sabatani, E.; Nikol, H. D.; Gray, H. B.; Anson, F. C. *J. Am. Chem. Soc.* **1996**, *118*, 1158. (d) Nair, R. B.; Cullum, B. M.; Murphy, C. J. *Inorg. Chem.* **1997**, *36*, 962.

10.1021/ic800753f CCC: $40.75
Published on Web 10/02/2008

switch is governed by a state reversal, with the emissive MLCT (phen) state lying lowest in energy in organic solvents resulting in luminescence. The energy of the MLCT (phz) state was believed to be sufficiently lowered in water for it to become the lowest lying state, which results in luminescence quenching.[5] Subsequent research has focused on the mechanism of the light switch effect. Variable temperature emission measurements[6] demonstrate that the light switch effect for $[Ru(bpy)_2(dppz)]^{2+}$ is not governed by a state reversal. The nonemissive ^{3}MLCT (phz) state has been proposed to be the lowest state in all solvents. However, it was stated that this state is also characterized by lower entropy and its population in organic solvents at ambient temperatures is reduced because of the dominance of $T\Delta S$.

The observed light switch behavior can be attributed to the competition between energetic factors favoring the dark ^{3}MLCT (phz) and entropic factors favoring the higher lying emissive ^{3}MLCT (phen) state.[6] The balance in the population of these two states can be changed by either temperature (affecting $T\Delta S$ term) or solvent (by changing the relative energy of the two states). In an aqueous environment at room temperature the energy of the dark ^{3}MLCT (phz) state is sufficiently low for the enthalpic term to dominate, resulting in the "switching off" of the emission.

Variable temperature emission measurements in polyol solvents have also provided the evidence for the existence of the dark lowest energy state.[7] This lowest state has been assigned to a doubly hydrogen bonded ^{3}MLCT (phz) state, and the next lowest state to a singly hydrogen bonded ^{3}MLCT (phz) state. The possibility that a ^{3}IL(π-π*) (phz) state may also be a dark state has also been suggested on the basis of density-functional theory (DFT) calculations.[8]

The properties of Redppz related complexes have attracted less attention than the analogous Ru and Os compounds. The Re^I complexes *fac*-[Re(α-*diimine*)$(CO)_3$Cl] (α-*diimine* = phen, bpy, *etc.*) are known to possess ^{3}MLCT lowest excited states.[9] The incorporation of the dppz ligand results in a more complicated excited-state manifold, and the assignment of the lowest excited states in these complexes can be less straightforward; ^{3}IL(π-π*), ^{3}MLCT (phen), and ^{3}MLCT (phz) states must be considered.[10] For example, the emission study of *fac*-$[Re(CO)_3(11,12\text{-}X_2\text{-dppz})(L)]^{0,+}$ [X = H, CH_3 and Cl; L = Cl, 4-ethylpyridine (4-Etpy), 4,4′-bipyridine (4,4′-bpy)] in solution at room temperature and MeTHF glasses has provided evidence for the presence of both ^{3}IL(π-π*) state and MLCT states.[10h]

Time-resolved vibrational spectroscopy is a powerful probe of excited-state structure. Time-resolved Raman spectroscopy has been used to probe the photophysics of a range of Redppz complexes by examining the fingerprint bands of the dppz ligand.[11] Time-resolved Infrared (TRIR) spectroscopic measurements have also proved useful for probing the nature of the excited states of metal carbonyl complexes, particularly for distinguishing between ^{3}IL(π-π*) and ^{3}MLCT states involving either phen or phenazine based orbitals, since the ν(CO) band energies are diagnostic of each of these states.[12] The shift of excited-state IR bands to lower wavenumber is characteristic to the formation of the ^{3}IL (π-π*) excited state, while ^{3}MLCT excited states results in a shift to higher wavenumber for the ν(CO) bands, a consequence of lower electron density at the metal center. The IR spectrum of the phz-based MLCT states possess ν(CO) bands which are shifted to higher wavenumber relative to the phen-based MLCT state, reflecting the lower electron density on the metal center in the phz-based MLCT state.[12]

In this paper we investigate the photophysics of *fac*-$[ReCl(CO)_3(11,12\text{-}X_2\text{-dppz})]$ [X = CH_3 (**1**), H (**2**), F (**3**), Cl (**4**), CF_3 (**5**)] by direct monitoring of the interplay between the three possible excited states with TRIR. We use spectroelectrochemical techniques (IR, UV/visible, and Electron Paramagnetic Resonance (EPR) spectroscopies) for this series of complexes to provide an insight into the ground-state electronic structure of these molecules and compare with the results of DFT calculations. We also report TRIR spectroscopic studies for **1**−**5** in a series of solvents of different polarity and hydrogen bonding ability, mirroring the changes inherent to the "light switch effect", to directly monitor the change in the population of both MLCT (phen) and MLCT (phz) excited states.

(5) Olson, E. J. C.; Hu, D.; Hormann, A.; Jonkman, A. M.; Arkin, M. R.; Stemp, E. D. A.; Barton, J. K.; Barbara, P. F. *J. Am. Chem. Soc.* **1997**, *119*, 11458.

(6) (a) Brennaman, M. K.; Alstrum-Acevedo, J. H.; Fleming, C. N.; Jang, P.; Meyer, T. J.; Papanikolas, J. M. *J. Am. Chem. Soc.* **2002**, *124*, 15094. (b) Brennaman, M. K.; Meyer, T. J.; Papanikolas, J. M. *J. Phys. Chem.* **2004**, *108*, 9938.

(7) (a) Olofsson, J.; Onfelt, B.; Lincoln, P. *J. Phys. Chem. A* **2004**, *108*, 4391. (b) Onfelt, B.; Olofsson, J.; Lincoln, P.; Norden, B. *J. Phys. Chem. A* **2003**, *107*, 1000. (c) Olofsson, J.; Wilhelmsson, L. M.; Lincoln, P. *J. Am. Chem. Soc.* **2004**, *126*, 15458.

(8) Pourtois, G.; Beljonne, D.; Moucheron, C.; Schumm, S.; Kirsch-De Mesmaeker, A.; Lazzaroni, R.; Bredas, J. L. *J. Am. Chem. Soc.* **2004**, *126*, 683.

(9) Giordano, P. J.; Wrighton, M. S. *J. Am. Chem. Soc.* **1979**, *101*, 2888.

(10) (a) Schoonover, J. R.; Strouse, G. F.; Chen, P. Y.; Bates, W. D.; Meyer, T. J. *Inorg. Chem.* **1991**, *32*, 2618. (b) Schoonover, J. R.; Strouse, G. F.; Dyer, R. B.; Bates, W. D.; Chen, P. Y.; Meyer, T. J. *Inorg. Chem.* **1996**, *35*, 273. (c) Yam, V. W. W.; Lo, K. K. W.; Cheung, K. K.; Kong, R. Y. C. *J. Chem. Soc., Dalton Trans.* **1997**, 2067–2072. (d) Cheung, K. K.; Kong, R. Y. C. *J. Chem. Soc., Chem. Commun.* **1995**, 1191. (e) Stoeffler, H. D.; Thornton, N. B.; Temkin, S. L.; Schanze, K. S. *J. Am. Chem. Soc.* **1995**, *117*, 7119. (f) Metcalfe, C.; Webb, M.; Thomas, J. A. *Chem. Commun.* **2002**, 2026. (g) Dyer, J.; Blau, W. J.; Coates, C. G.; Creely, C. M.; Gavey, J. D.; George, M. W.; Grills, D. C.; Hudson, S.; Kelly, J. M.; Matousek, P.; McGarvey, J. J.; McMaster, J.; Parker, A. W.; Towrie, M.; Weinstein, J. A. *Photochem. Photobiol. Sci.* **2003**, *2*, 542. (h) López, R.; Loeb, B.; Striplin, D.; Devenney, M.; Omberg, K.; Meyer, T. J. *J. Chil. Chem. Soc.* **2004**, *49*, 149. (i) Kuimova, M. K.; Grills, D. C.; Matousek, P.; Parker, A. W.; Sun, X. Z.; Towrie, M.; George, M. W. *Vibr. Spectrosc.* **2004**, *35*, 219. (j) Ruiz, G. T.; Juliarena, M. P.; Lezna, R. O.; Wolcan, E.; Feliz, M. R.; Ferraudi, G. *Dalton Trans.* **2007**, 2020. (k) Foxon, S. P.; Phillips, T.; Gill, M. R.; Towrie, M.; Parker, A. W.; Webb, M.; Thomas, J. A. *Angew. Chem.* **2007**, *46*, 3686.

(11) (a) Waterland, M. R.; Gordon, K. C.; McGarvey, J. J.; Jayaweera, P. M. *J. Chem. Soc., Dalton Trans.* **1998**, 609. (b) Waterland, M. R.; Gordon, K. C. *J. Raman Spectrosc.* **2000**, *31*, 243. (c) Walsh, P. J.; Gordon, K. C.; Lundin, N. J.; Blackman, A. G. *J. Phys. Chem. A,* **2005**, *109*, 5933.

(12) (a) Kuimova, M. K.; Alsindi, W. Z.; Dyer, J.; Grills, D. C.; Jina, O. S.; Matousek, P.; Parker, A. W.; Portius, P.; Sun, X. Z.; Towrie, M.; Wilson, C.; Yang, J. X.; George, M. W. *Dalton Trans.* **2003**, 3996. (b) Kuimova, M. K.; Sun, X. Z.; Matousek, P.; Grills, D. C.; Parker, A. W.; Towrie, M.; George, M. W. *Photochem. Photobiol. Sci.* **2007**, *6*, 1158.

Experimental Section

Dichloromethane and acetonitrile (Fisher, HPLC grade) were distilled under an atmosphere of dinitrogen from calcium hydride. Butyronitrile, propionitrile, propanol and methanol (HPLC grade), 1,10-phenanthroline-5,6-dione, 1,2-diamino-4,5-dimethylbenzene (Aldrich), [ReCl(CO)$_5$] (Alfa Aesar), 1,2-diamino-4,5-dichlorobenzene, 1,2-diamino-4,5-difluorobenzene (Fluorochem), 1,2-diamino-4,5-di(tetrafluoromethyl)chlorobenzene (Interchim) were used as received. Silica (Fluorochem, 60 A, 35−70 μm) was used for column chromatography. *fac*-[ReCl(CO)$_3$(phen-5,6-dione)] was synthesized according to a literature procedure,[10e] and *fac*-[ReCl(CO)$_3$(dppz-X$_2$)], [X = CH$_3$ (**1**), H (**2**) F (**3**), Cl (**4**), CF$_3$ (**5**)] were synthesized by adaptation of the methods reported for similar complexes.[10e] The purity of the compounds was confirmed by ^{1}H NMR and FTIR spectroscopies. *fac*-[ReCl(CO)$_3$(dppz-(CF$_3$)$_2$)] (**5**) Found: C, 38.05; H, 1.06; N, 7.43. $C_{23}H_8ClN_4F_6O_3Re$ requires C, 38.16; H, 1.11; N, 7.74%; ν_{max}/cm^{-1} (CO) 2025, 1924, 1903.5 (CH_2Cl_2); ^{1}H NMR (300 MHz; $CDCl_3$): δ 8.11 (2 H, dd, 5.1 Hz, 8.1 Hz, H-2 and H-7), 9.03 (2 H, s, H-10 and H-13), 9.55 (2 H, dd, 1.5 Hz, 5.1 Hz, H-1 and H-8) and 9.87 (2 H, dd, 1.5 Hz, 8.1 Hz, H-3 and H-6); ^{19}F NMR (282 MHz; $CDCl_3$): δ 58.62 (CF_3); *m*/*z* (ES) 724 (M^+). The spectroscopic data (^{1}H NMR, FTIR) for **1**, **2**, **3**, and **4** are consistent with those reported previously. Additional purification for emission measurements by column chromatography (silica, THF as eluent, first fraction collected) was also performed. Crystals of *fac*-[ReCl(CO)$_3$(dppz-(CH$_3$)$_2$)] (**1**) were grown by slow diffusion of ether into a CH_2Cl_2 solution. The molecular structures of **1**, **3**, and **4** determined by X-ray crystallography are shown below (atomic displacement ellipsoids are drawn at the 50% probability level), Figure 1.[13] In the crystal structure of *fac*-[ReCl(CO)$_3$(dppz-(CH$_3$)$_2$)] (**1**), the metal center possesses a distorted octahedral geometry. The equatorial Re−CO distances of 1.918(4) and 1.929(4) Å which lie *trans* to N atoms [Re−N 2.180(3), 2.189(3) Å] are significantly shorter than the axial Re−CO distance of 2.006(5) Å which lies opposite a chloride ligand [Re−Cl 2.4755(11) Å]. The principal angular distortion from ideal octahedral geometry is seen in the N−Re−N angle of 75.15(11)° and arises from the small bite angle of the phenazine ligand. The ReC_2N_2 equatorial plane is inclined by a significant extent [11.81(4)°] to the plane of the phenazine ligand, imparting a visible curvature to the complex such that the metal center lies 0.324(1) Å out of the plane of the phenazine ligand. The heavy-atom skeleton of the phenazine ligand is only approximately planar (rms deviation 0.063 Å) and can also be visualized as a series of more nearly planar rings inclined to each other by up to 4.6°.

In the crystal structure of *fac*-[ReCl(CO)$_3$(dppz-F$_2$)] (**3**), the metal center also possesses a distorted octahedral geometry. The equatorial Re−CO distances of 1.925(5) and 1.926(5) Å which lie *trans* to N atoms [Re−N 2.169(4), 2.180(4) Å] are shorter than the axial Re−CO distance of 1.952(6) Å which lies opposite a chloride ligand [Re−Cl 2.4777(12) Å]. The N−Re−N angle of 75.73(14)° is slightly wider than the values in (**1**) and (**4**). The molecule is strongly bowed, with a dihedral angle of 31.3(2)° between the ReC_2N_2 equatorial plane and the plane of the most remote C9−C14 ring of the phenazine ligand. The metal center is displaced from the local C_2N_2 plane by 0.087(2) Å in the direction of the axial CO group.

In the crystal structure of *fac*-[ReCl(CO)$_3$(dppz-Cl$_2$)] (**4**), the metal center also possesses a distorted octahedral geometry. The equatorial Re−CO distances of 1.906(5) and 1.924(4) Å which lie *trans* to N atoms [Re−N 2.170(3), 2.191(3) Å] bracket the axial Re−CO distance of 1.919(5) Å which lies opposite a chloride ligand [Re−Cl 2.4766(11) Å]. The N−Re−N angle of 75.17(12)° is almost identical to the value in (**1**). The ReC_2N_2 equatorial plane and the plane of the phenazine ligand are inclined by 11.45(8)°, and the metal center lies 0.340(1) Å from the plane of the phenazine ligand. The rms deviation from the least-squares mean plane through the phenazine (0.056 Å) again indicates the limited planarity of the complete ligand.

The samples for emission and (spectro)electrochemical measurements were prepared with distilled solvents, which were further degassed and purged with Ar to remove dissolved oxygen. Solutions for the electrochemical experiments contained either 0.2 M (in CH_3CN) or 0.4 M (in CH_2Cl_2) of [NBu$_4$][BF$_4$] as supporting electrolyte. Cyclic voltammetric studies were carried out using an EG&G Instruments Model 362 scanning potentiostat with a three-electrode arrangement in a single compartment cell. A Pt working and secondary electrode, and a Ag/AgCl reference electrode, chemically isolated from the test solution via a bridge tube containing electrolyte solution and fitted with a glass frit, were used in the cell. The concentration of the test compounds was 10^{-3} M. Redox potentials are quoted versus $E_{1/2}$ ferrocenium-ferrocene (F_c+/F_c) couple which was used as an internal reference. Compensation for internal resistance was not applied. In situ UV/visible and FTIR spectroelectrochemical experiments were carried out at an optically transparent electrode OTE (UV/visible) or an optically transparent thin-layer electrochemical (OTTLE) cell (IR). For UV/visible studies, the cell consisted of a modified quartz cuvette (optical path length: 0.5 mm) and three-electrode configuration; a Pt/Rh gauze working electrode, a Pt wire secondary electrode (in a fritted PTFE sleeve), and a saturated calomel electrode, chemically isolated from the test solution via a bridge tube containing electrolyte solution and terminated in a porous frit. The potential at the working electrode was controlled by a Sycopel Scientific Ltd. DD10 M potentiostat. The UV/visible spectra were recorded on a Perkin-Elmer Lambda 16 spectrophotometer. The cavity was purged with dinitrogen and temperature control at the sample was achieved by flowing cooled dinitrogen across the surface of the cell. For FTIR experiments the cell consisted of a modified solution cell (Specac) (optical path length: 200 μm) equipped with CaF_2 windows and three-electrode configuration; Pt/Rh minigrid working and (unbridged) secondary electrodes and a twisted Ag wire pseudoreference electrode. The cell was positioned so that the beam passed through the center of the working electrode; all other electrodes were masked. Potentials were controlled by an Autolab PGSTAT20 potentiostat and spectra were recorded at ambient temperature on a Nicolet AVATAR FTIR spectrometer. For UV/visible and FTIR spectroelectrochemical studies the test species in solution was electrolyzed at constant potential, typically 80 mV more positive than E_p^a for an oxidation experiment and 80 mV more negative than E_p^c for a reduction. The redox process was considered complete

(13) (a) Crystal data for **1**, $C_{23}H_{14}ClN_4O_3Re\cdot{}^1/_2CH_2Cl_2$, M = 658.49, monoclinic, space group *I*2/*a* (*alt*. *C*2/*c*, No. 15), a = 13.5854(10), b = 18.1464(13), c = 18.5411(13) Å, β = 104.632(1)°, U = 4422.6(9) Å^3, Z = 8, D_c = 1.978 Mg/m^3, μ(Mo-Kα) = 5.772 mm^{-1}, T = 150(2) K; 5063 unique reflections (R_{int} = 0.048). Final R_1 [4526 $I > 2\sigma(I)$] = 0.0265, wR_2 (all data) = 0.0760,(b) Crystal data for **3**, $C_{21}H_8ClF_2N_4O_3Re$, M = 623.96, monoclinic, space group $P2_1/n$ (*alt.* $P2_1/c$, No. 14), a = 6.4966(2), b = 23.2065(6), c = 12.7762(3) Å, β = 97.7463(15)°, U = 1908.61(9) Å^3, Z = 4, D_c = 2.171 Mg/m^3, μ(Mo-Kα) = 6.560 mm^{-1}, T = 120(2) K; 4378 unique reflections (R_{int} = 0.046). Final R_1 [3975 $I > 2\sigma(I)$] = 0.0312, wR_2 (all data) = 0.0654, and (c) Crystal data for **4**, $C_{21}H_8Cl_3N_4O_3Re\cdot{}^1/_2C_4H_8O$, M = 692.92, monoclinic, space group *C*2/*c* (No. 15), a = 19.958(2), b = 18.054(2), c = 13.530(2) Å, β = 116.562(2)°, U = 4360.5(15) Å^3, Z = 8, D_c = 2.111 Mg/m^3, μ(Mo-Kα) = 5.980 mm^{-1}, T = 150(2) K; 4906 unique reflections (R_{int} = 0.024). Final R_1 [4176 $I > 2\sigma(I)$] = 0.0261, wR_2 (all data) = 0.0722.

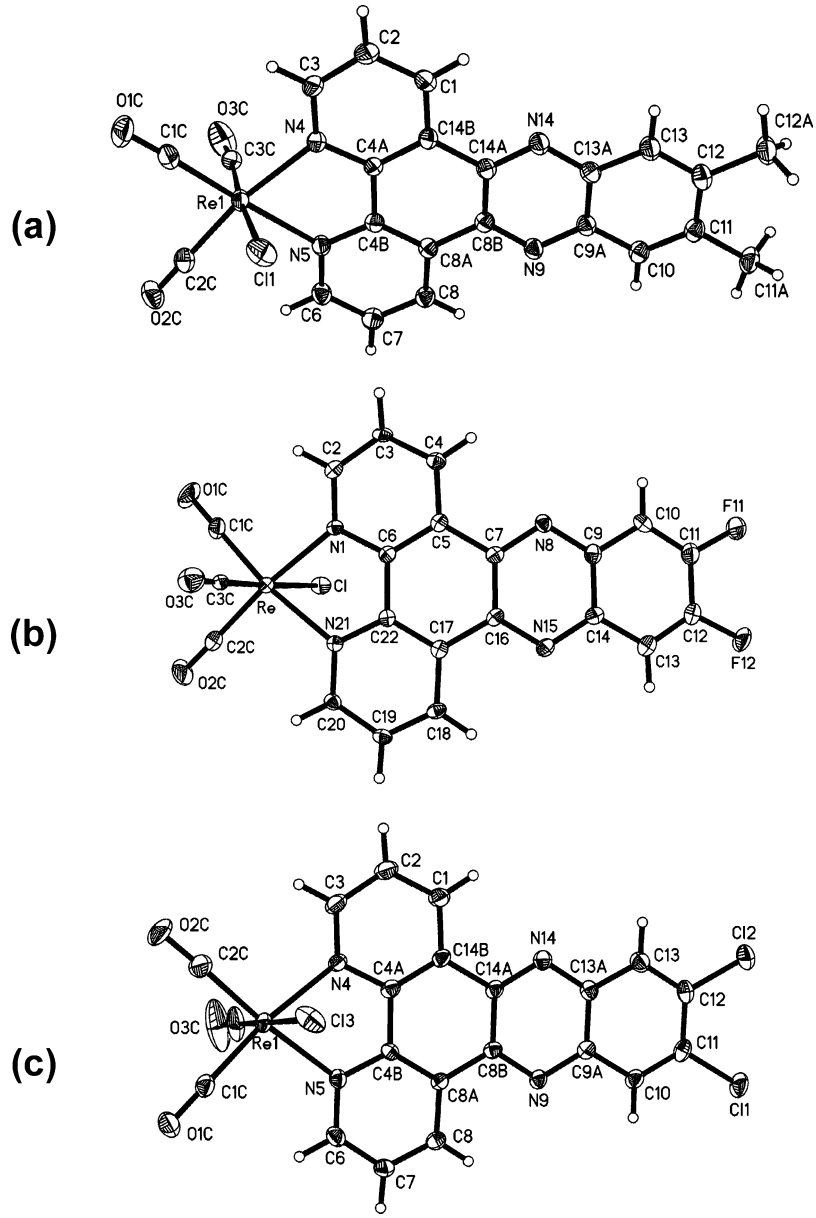

Figure 1. Displacement ellipsoid plot drawing of (a) *fac*-[ReCl(CO)$_3$(dppz-(CH$_3$)$_2$)] (**1**), (b) *fac*-[ReCl(CO)$_3$(dppz-F$_2$)] (**3**), and (c) *fac*-[ReCl(CO)$_3$(dppz-Cl$_2$)] (**4**) with 50% probability displacement ellipsoids. The CH_2Cl_2 and THF solvent molecules in **1** and **4** are omitted for clarity.

when consecutive spectra were identical. The chemical reversibility of the process was investigated by applying a potential at the working electrode sufficient to reoxidize or rereduce the electrogenerated product. These potentials were typically >100 mV more negative than E_p^c to reverse an oxidation process or >100 mV more positive than E_p^a to reverse a reduction process. The process was considered to be reversible, under the conditions of the experiment, if the spectroscopic profile of the starting material was reproduced.

Coulometric studies (at controlled potential) were carried out using an Autolab PGSTAT20 potentiostat and a two-compartment cell. The Pt/Rh gauze basket working electrode was separated from the wound Pt/Rh gauze secondary electrode by a glass frit. A saturated calomel reference electrode was bridged to the test solution through a Vycor frit orientated at the center of the working electrode. The working electrode compartment was fitted with a magnetic stirrer bar, and the test solution was stirred rapidly during electrolysis. Electrolyzed solutions were transferred via cannula to an airtight quartz tube for EPR studies. EPR spectra were recorded on a Bruker EMX spectrometer. Simulated EPR spectra were obtained with WINEPR SimFonia v1.25.

DFT geometry optimizations on *fac*-[ReCl(CO)$_3$(dppz-X$_2^{\bullet-}$)] and *fac*-[ReCl(CO)$_3$(dppz-X$_2$)] (X = CH_3, H, F, Cl, CF_3) were performed using the ADF2004 suite of programs[14,15] running on a SGI O2 RS12000 computer or Dell Linux 2-processor system in restricted and unrestricted modes, respectively. Singlet → singlet/triplet time-dependent DFT (TDDFT) calculations were performed on calculated geometries for *fac*-[Re(CO)$_3$(dppz-X$_2$)Cl] (X = CH_3, H, F, Cl, CF_3) to gain insight into the energies of the excited states of these complexes. The calculations were performed under C_s symmetry using a coordinate frame where the *yz* plane contains the Re and Cl atoms, and bisects the N−Re−N angle that the dppz ligand makes at the Re center, Scheme 1.

(14) Baerends, E. J.; Ellis, D. E.; Ros, P. *Chem. Phys.* **1973**, *2*, 41.
(15) Velde, G. T.; Baerends, E. J. *J. Comput. Phys.* **1992**, *99*, 84.

Scheme 1. Schematic Diagram of *fac*-[ReCl(CO)$_3$(dppz-X$_2$)] X = CH$_3$ (**1**), H (**2**), Cl (**3**), F (**4**), CF$_3$ (**5**)

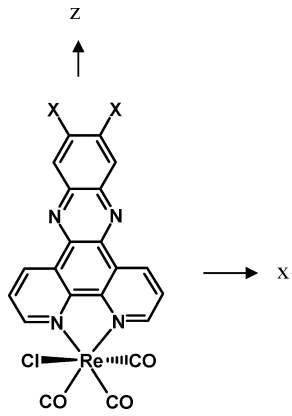

The DFT calculations employed Slater type orbital (STO) triple-ζ-plus polarization basis sets (from the TZP database of the ADF suite), the frozen core approximation (up to and including 4d for Re and 1s for C, N, and O), and the local density approximation (LDA) with the correlation potential due to Vosko et al. (VWN).[16] Gradient corrections were performed using the functionals of Becke[17] and Perdew (BP).[18] A scalar relativistic zero order regular approximation (ZORA) was used for the inclusion of relativistic effects. The conductor-like screening model (COSMO) was used to estimate the effect of a solvent with a dielectric constant of 37.5 on the electronic structure. The program MOLEKEL[19] was used to prepare three-dimensional plots of the electron density.

Emission measurements were performed on an Edinburgh Instruments FLS920 combined fluorescence lifetime and steady state spectrometer. The optical density was adjusted to about 0.2−0.3 at the excitation wavelength. Steady state emission and excitation spectra were obtained with a xenon arc lamp as the excitation source and were corrected for detector sensitivity. Emission quantum yields, ϕ_{em} were determined using a solution of [Ru(bpy)$_3$]Cl$_2$ in D$_2$O as the emission standard.[20]

The picosecond TRIR experiments were carried out on the PIRATE apparatus at the Central Laser Facility of the STFC Rutherford Appleton Laboratory. This apparatus has been described in detail previously.[21] Part of the output from a 1 kHz, 800 nm, 150 fs, 1 mJ Ti-Sapphire oscillator/regenerative amplifier (Spectra Physics Tsunami/Spitfire) was used to pump a white light continuum seeded β-BaB$_2$O$_4$ (BBO) optical parametric amplifier (OPA). The signal and idler produced by this OPA were difference frequency mixed in a type I AgGaS$_2$ crystal to generate tuneable mid-infrared pulses (ca. 150 cm^{-1} fwhm, 1 μJ), which were split to give probe and reference pulses. Second harmonic generation of the residual 800 nm light provided 400 nm pump pulses. Both the pump and probe pulses were focused to a diameter of 200−300 μm in the sample. Changes in infrared absorption at various pump−probe time delays were recorded by normalizing the outputs from a pair of 64-element MCT infrared linear array detectors on a shot-by-shot basis. In all TRIR experiments dry, degassed solutions were saturated with argon and flowed through a home-built flow system incorporating an IR cell (Harrick Scientific Corp.) and a recirculating pump (Micropump) or Teflon peristaltic pump (Cole Palmer).

Fitting of the ps-TRIR spectra was performed in ORIGIN 7.2 (OriginLab, Northampton, MA) using the sum of Lorentzian bands. To allow a precise determination of position and intensity of transient bands in the TRIR spectra, the fitting parameters of the ground-state bands were independently obtained from the ground-state IR absorbance spectra. The Lorentzian band parameters (band positions, widths, and the ratio between the band areas), obtained from the ground-state IR, were fixed during the fit of the ps-TRIR spectra. In the 1900−2000 cm^{-1} spectral region fitting of the spectra to more than one excited state was complicated. Therefore the minimum number of Lorentzian bands was employed and no attempt was made to distinguish between the MLCT (phen) and MLCT (phz) features.

Results and Discussion

Electrochemistry of *fac*-[ReCl(CO)$_3$(dppz-X$_2$)] (1−5). The electrochemical properties of **1**−**5** were studied in CH$_2$Cl$_2$ using cyclic voltammetry, Table 1.[22] The potentials of the first reduction potentials, E_{red1}, for **1**, **2**, **4** were consistent with those of previous studies.[11a,b] The value of E_{red1} was strongly dependent on the nature of the substituent on the phz fragment of the dppz ligand (X) with the more electron withdrawing substituents leading to less negative values of E_{red1}.[23] The UV/visible spectra obtained following in situ reduction of **1**−**5** were also consistent with previous results.[24] The typical changes in the UV/visible spectra following one electron reduction of **5** are shown in Figure 2a. Similar changes are also observed for **2** and **4** and are consistent with those reported previously, Table 1.[11a] On the basis of these data and previous findings[2] for *fac*-[ReCl(CO)$_3$(dppz)] and [M(bpy)$_2$(dppz)]$^{2+}$, M = Ru^{II}, Os^{II}, we conclude that the first one electron reduction process is localized predominantly on the phz unit of dppz.

Further information can be obtained from the IR spectral changes accompanying the one electron reduction of *fac*-[ReCl(CO)$_3$(dppz-X$_2$)] (e.g., Figure 2, b for **5**). Three new ν(CO) bands appear at lower wavenumber (ca. 10 cm^{-1}) relative to the parent bands following reduction of the parent compounds (Table 1), and this shift was considerably less than the corresponding shift observed for *fac*-[ReCl(CO)$_3$(α-*diimine*)], (α-*diimine* = substituted bpy or phen) (ca. 30 cm^{-1}).[25] The smaller shift of 10 cm^{-1} is consistent with the

(16) Vosko, S. H.; Wilk, L.; Nusair, M. *Can. J. Phys.* **1980**, *58*, 1200.
(17) Becke, A. D. *Phys. Rev. A* **1988**, *38*, 3098.
(18) Perdew, J. P. *Phys. Rev. B* **1986**, *33*, 8822.
(19) Portmann, S.; Luthi, H. P. *Chimia* **2000**, *54*, 766.
(20) Caspar, J. V.; Meyer, T. J. *J. Am. Chem. Soc.* **1983**, *105*, 5583.
(21) Towrie, M.; Grills, D. C.; Dyer, J.; Weinstein, J. A.; Matousek, P.; Barton, R.; Bailey, P. D.; Sabramaniam, N.; Kwok, W. M.; Ma, C.; Phillips, D.; Parker, A. W.; George, M. W. *Appl. Spectrosc.* **2003**, *57*, 367.

(22) Each complex displayed two cathodic reductions and one anodic oxidation processes. The first cathodic reduction process (E_{red1}) is a one electron process, as determined by coulometry. E_{red1} is a thermodynamically reversible Nernstian process. However, the second cathodic reduction (E_{red2}) and anodic oxidation (E_{ox}) are chemically irreversible.

(23) The E_{red1} values correlate linearly with the Hammett parameters for the substituent X.

(24) The UV/visible spectra of **1**−**5** are dominated by the intense IL(π-π*) transitions centred around 250−380 nm. The structured band centred at 340−400 nm is characteristic of an IL(π-π*) transition of the dppz ligand. These bands and the higher-lying phen-like IL(π-π*) transitions (ca. 300 nm) increase in energy with the increase in acceptor ability of X. The lower energy broad band at about 420 nm, which appears as shoulder under the characteristic dppz IL(π-π*) structured band, becomes more prominent as the acceptor ability of X increases and this band is assigned to the MLCT (phen) transition.

(25) (a) Johnson, F. P. A.; George, M. W.; Hartl, F.; Turner, J. J. *Organometallics* **1996**, *15*, 3374. (b) Howell, S. L.; Gordon, K. C. *J. Phys. Chem. A* **2006**, *110*, 4880.

Table 1. (Spectro)Electrochemical Data (Cyclic Voltammetry,[a] UV/visible,[b,c] IR[b]) for *fac*-[ReCl(CO)$_3$(dppz-X$_2$)] Recorded in CH_2Cl_2, 0.4 M $(Bu_4N)BF_4$ As Supporting Electrolyte at Room Temperature

X	$E_{ox}(E_p^c - E_p^a)$	E_{red1} $(E_p^c - E_p^a)$	E_{red2} $(E_p^c - E_p^a)$	parent species: λ/nm ($\varepsilon \times 10^{-3}$/cm^{-1} M^{-1})[c]	reduced species: λ/nm ($\varepsilon \times 10^{-3}$/cm^{-1} M^{-1})[c]	ν(CO)/cm^{-1} neutral	ν(CO)/cm^{-1}, 1e-reduced
CH_3	0.96[d]	−1.48 (0.08)	−2.05 (0.10)	298 (60), 374 (15), 391 (16), 382 (10), 358 (12)	230 (33), 261 (36), 299 (27), 341 (28), 353 (28), 399 (14), 458 (6), 498 (4), 570 (sh), 605 (11)	2025, 1923, 1903	2019, 1911, 1895
H	0.92[e]	−1.42[e]	−2.00[e]	280 (60), 322 (14), 376 (16), 394 (13)	229 (30), 259 (38), 297 (27), 344 (27), 389 (12), 452 (5), 494 (4), 560 (sh), 589 (11)	2024, 1921, 1900	2017, 1909, 1892
F	1.02[d]	−1.32 (0.08)	−1.68 (0.08)	262 (sh), 276 (54), 319 (14), 360 (11), 380 (9), 400 (sh)	232 (30), 250 (32), 291 (26), 335 (22), 391 (11), 446 (5), 568 (6), 600 (9)	2024, 1921, 1900	2018, 1910, 1893
Cl	1.06[d]	−1.24 (0.06)	−1.87 (0.06)	282 (68), 322 (14), 375 (16)	231 (30), 262 (37), 283 (34), 297 (sh), 342 (27), 374 (14), 397 (13), 460 (5), 495 (4), 566 (8), 605 (12)	2025, 1923, 1901	2017, 1910, 1892
CF_3	1.03[d]	−1.05 (0.06)	−1.77 (0.06)	265 (65), 273 (77), 297 (27), 315 (18), 343 (12), 357 (13), 400 (sh)	256 (40), 292 (31), 335 (34), 382 (11), 442 (7), 547 (9), 587 (12)	2025, 1924, 1904	2018, 1911, 1895

[a] Potentials in V vs Ferrocenium/Ferrocene, separations ($E^c - E^a$) in V at 0.1 Vs^{1-}. [b] Recorded at an OTTLE. [c] UV/visible data recorded at ca. 273 K. [d] Peak potential for irreversible process. [e] from ref 2a, in CH_3CN.

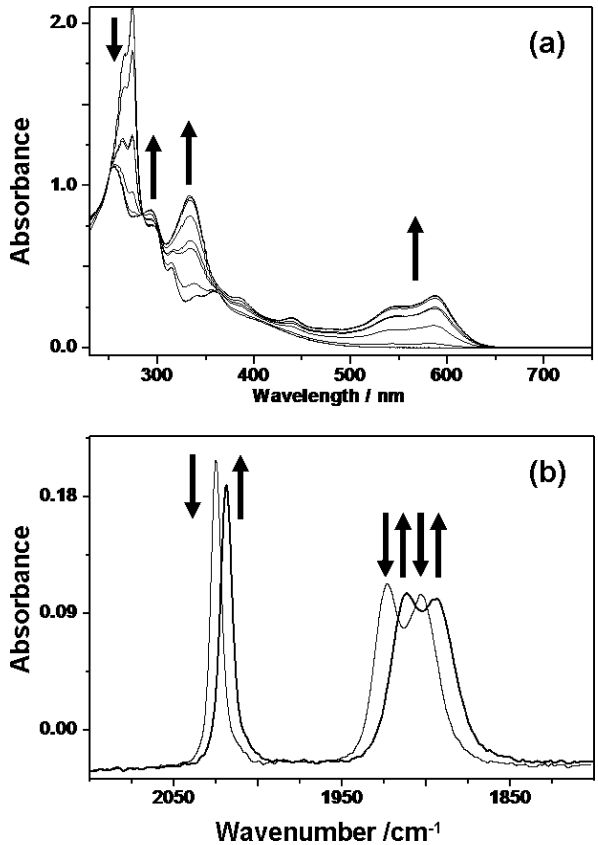

Figure 2. (a) UV/visible and (b) IR spectra recorded following the one electron reduction of *fac*-[ReCl(CO)$_3$(dppz-(CF$_3$)$_2$)] in CH_2Cl_2, 0.4 M $(Bu_4N)BF_4$.

electron occupying a phz orbital on dppz, since in the case of phz-based reduction there is considerably less backbonding to the Re center, compared to the product of phen-based reduction.

More detailed information regarding the nature of the singly occupied molecular orbital (SOMO) of reduced *fac*-[ReCl(CO)$_3$(dppz-X$_2$)] was obtained from EPR spectroscopy. The parent compounds were found to be EPR silent. The reduced complexes display EPR spectra with g values about 2.004 (Table 2), very close to that of free electron, $g = 2.0023$. These spectra showed significant ligand hyperfine structure (Figure 3). No metal hyperfine structure from ^{187}Re ($I = 5/2$, 62.6%) or ^{185}Re ($I = 5/2$, 37.4%) was observed. These spectra were consistent with those observed previously[2] for *fac*-[ReCl(CO)$_3$(dppz)] and can be simulated using a sum of Gaussian shape lines, resulting from interactions of the unpaired electron with spin-active nuclei on the dppz ligand (Table 2). For one electron reduced *fac*-[ReCl(CO)$_3$-(dppz-X$_2$)] (X = CH_3, H, Cl) the EPR spectra may be considered to consist of five lines which are in turn split by further hyperfine coupling. The major coupling (leading to the five lines) results from the interaction of the unpaired electron with a pair of equivalent N atoms, $a_{2N} \approx 5$ G. In addition, to model the pattern of the hyperfine couplings and the intensities in the spectra for X = H and Cl, two relatively large a_H with the two pairs of H atoms (Table 2) are required to simulate this data. For *fac*-[ReCl(CO)$_3$(dppz-(CH$_3$)$_2$)] the shape of the EPR spectrum differs from that of *fac*-[ReCl(CO)$_3$(dppz)] and required an additional coupling (a_H = 1.2 G) with six H atoms from methyl groups to reproduce the shape of experimental spectrum. For *fac*-[ReCl(CO)$_3$(dppz-F$_2$)] in addition to the major coupling with 2N nuclei, a pair of equivalent hyperfine couplings with two equivalent F atoms, which are comparable in magnitude to the main $a_{2N} \approx 5$ G, had to be included into the simulation to account for the spectral shape. Similarly, for one electron reduced *fac*-[ReCl(CO)$_3$(dppz-(CF$_3$)$_2$)] coupling to six equivalent atoms,

Table 2. Hyperfine Coupling Constants (Gauss) and *g* Values for One Electron Reduced *fac*-[ReCl(CO)$_3$(dppz-X$_2$)] from the Simulation of the EPR Spectra (and Calculated from the Electron Density)[a]

atom[b]/X	CH_3	H	F	Cl	CF_3
N1	5.0 (5.8)	4.93 (6.03)	4.95 (6.5)	4.87 (6.5)	5.1 (6.86)
N2	0.4 (0.49)	0.4 (0.44)	0.4 (0.12)	0.4 (0.08)	*d* (0.12)
H2	1.6 (1.8)	1.5 (1.75)	1.55 (1.2)	1.9 (1.2)	0.6 (0.58)
H4	1.45 (1.64)	1.45 (1.63)	1.2 (2.0)	0.7 (2.1)	2.63 (3.3)
X5	1.2[c] (1.02)	0.75 (0.8)	4.1 (2.19)		2.63 (*e*)
H3	0.75 (−0.83)	*d* (−0.82)	0.7 (−0.59)	*d* (−0.59)	*d* (−0.17)
H1	0.38 (−0.26)	0.38 (−0.21)	0.38 (0.09)	0.38 (0.12)	*c* (0.42)
g_{iso}	2.0035	2.0037	2.0036	2.0036	2.0037

[a] Hyperfine coupling constants were calculated from DFT calculation data according to the equation $a = Q\rho$, where $Q_N = 2.75$; $Q_H = 2.3$; $Q_{H\beta} = 5.38$; $Q_{F\beta} = 2.69$ and ρ is calculated electron density on either N atom or neighboring C atom.[41] [b] The numbering of the atoms is shown in Figure 3. [c] $a_{H\beta}$. [d] Not required. [e] $a_{F\beta}$, can not be calculated due to unknown $Q_{F\beta}$.

comparable in magnitude to the major a_{2N}, is required to obtain a good fit.

The EPR spectra shown in Figure 3 should be contrasted with the EPR spectra obtained following the one electron reduction of [ReCl(CO)$_3$(bpy)],[26] where the unpaired electron is occupying an orbital localized on the bpy ligand, and broad structureless EPR spectra are observed, due to the interactions of the unpaired electron with the metal. The large spin−orbit coupling induced by significant contribution from the metal ($\zeta_{Re} > 2000$ cm^{-1})[27] also results in a considerably smaller *g* value for the radical, typically <2.[28,29] The *g* values for one electron reduced **1**−**5** and the presence of highly resolved hyperfine structure is consistent with population of a phz-based orbital, which has minimal coupling to the metal center, and therefore experiences only slight perturbation from the metal atom.

The calculated energies and composition of the SOMOs of singly reduced *fac*-[ReCl(CO)$_3$(dppz-X$_2^{\bullet-}$)] in the gas phase have been determined (see Supporting Information), and the three-dimensional plots of the electron density for SOMOs in **1**−**5** are shown in Figure 3. It is clear that each SOMO possesses π-symmetry and is predominantly of phz character. The relative energy of the SOMO decreases with increasing electron withdrawing ability of the substituent on the dppz ligand.[30]

The spin densities on the dppz ligand nuclei obtained from the DFT calculations were used to calculate[31] the hyperfine coupling constants of *fac*-[ReCl(CO)$_3$(dppz-X$_2$)], and the trends observed in the calculated hyperfine coupling constants are consistent with those obtained from the simulation of the experimental EPR spectra (Table 2). This further supports

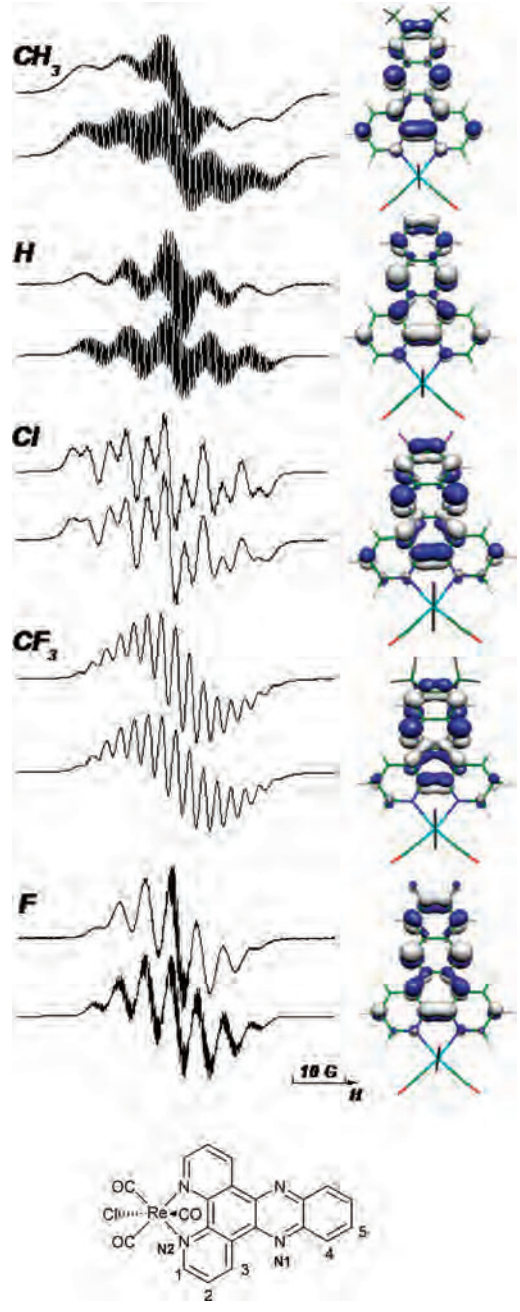

Figure 3. EPR spectra of one electron reduced *fac*-[ReCl(CO)$_3$(dppz-X$_2$)] (top) together with the simulated spectra (bottom) obtained using parameters listed in Table 2. The three-dimensional plots of the electron density for the DFT-calculated SOMO (gas phase) are shown on the right, the corresponding energies and orbital compositions are given in the Supporting Information.

(26) (a) Kaim, W.; Kohlmann, S. *Chem. Phys. Lett.* **1987**, *139*, 365–369. (b) Klein, A.; Vogler, C.; Kaim, W. *Organometallics* **1996**, *15*, 236–244.
(27) Schafer, R.; Kaim, W.; Moscherosch, M.; Krejcik, M. *J. Chem. Soc., Chem. Commun.* **1992**, 834.
(28) Collison, D.; Mabbs, F. E.; McInnes, E. J. L.; Taylor, K. J.; Welch, A. J.; Yellowlees, L. J. *J. Chem. Soc., Dalton Trans.* **1996**, 329.
(29) Mabbs, F. E.; Collison, D. *Electron Paramagnetic Resonance of d Transition Metal Compounds*; Elsevier: Amsterdam, 1992.
(30) The calculated LUMO energy for *fac*-[Re(Cl)(CO)$_3$(dppz-F$_2$)] is lower than that of *fac*-[Re(Cl)(CO)$_3$(dppz-Cl$_2$)], in spite of the stronger electron withdrawing ability of Cl vs F. This is probably due to overestimation in the stabilization effect of p/s overlap for fluorine in our DFT calculations.
(31) EPR hyperfine coupling constants for *fac*-[Re(Cl)(CO)$_3$(dppz-X$_2$)] were calculated from McConnell equation[41] which provides estimates of the hyperfine coupling constants (*a*) from the calculated spin density on either the N atom or the neighboring C atom (*r*): $a = Q^*r$, where $Q_N = 2.75$; $Q_H = 2.3$; $Q_{H\beta} = 5.38$; $Q_{F\beta} = 2.69$.

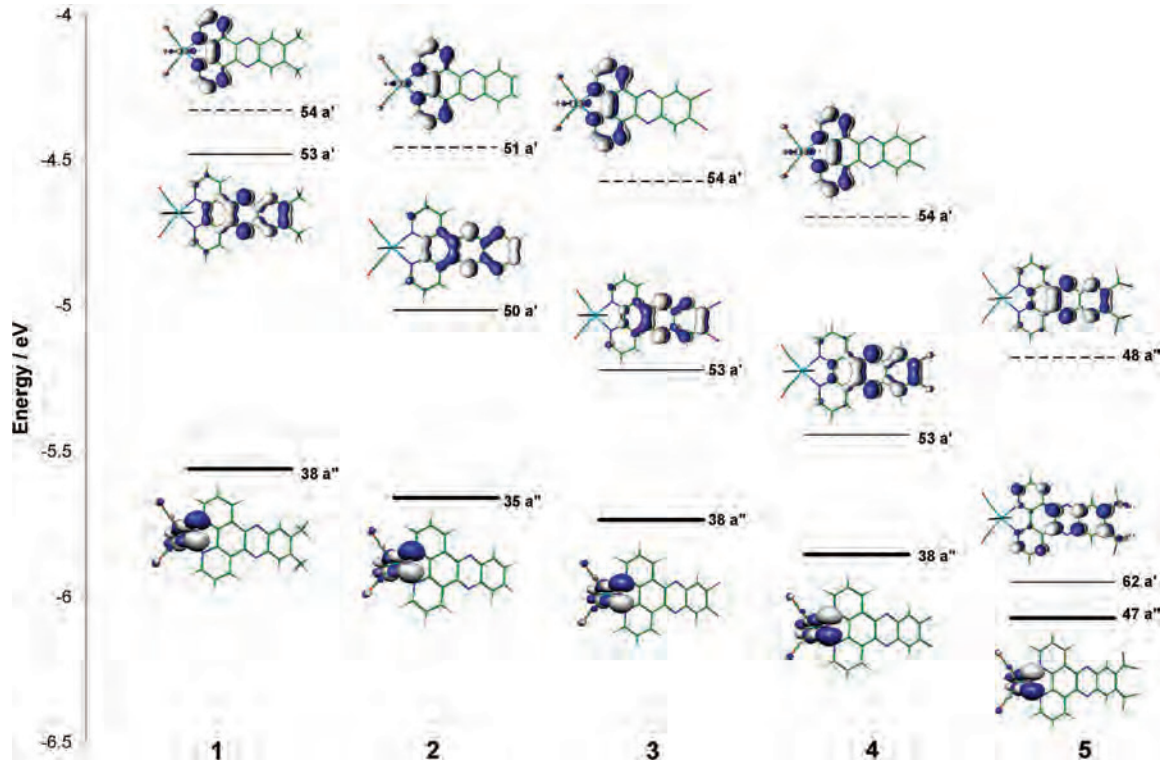

Figure 4. Partial energy level diagram for *fac*-[ReCl(CO)$_3$(dppz-X$_2$)], X = CH$_3$ (**1**), H (2), Cl (**3**), F (**4**), CF$_3$ (**5**) calculated in its ground state in the gas phase and three-dimensional plots of the electron density for the HOMO (thick solid line), LUMO (thin solid line), and LUMO+1 (dashed line).

the assignment of the SOMO occupied following one electron reduction of *fac*-[ReCl(CO)$_3$(dppz-X$_2$)] to the π symmetry orbital of phz character.

DFT Calculations and Photophysics of fac-[ReCl(CO)$_3$(dppz-X$_2$)] (1−5). We have used DFT calculations to determine the nature of the frontier orbitals in **1**−**5**. The calculated ordering of the frontier molecular orbitals of **1**−**5** in their ground states in the gas phase are shown in the partial energy level diagram (Figure 4), together with three-dimensional plots of the electron density for the highest occupied molecular orbital (HOMO), lowest unoccupied molecular orbital (LUMO), and LUMO+1.[32] The three HOMOs in **1**−**5** both in the gas phase and in a dielectric medium are predominantly metal based (dπ) and contain significant CO (π*) character from the equatorial and axial CO ligands. The lowest unoccupied molecular orbital is of π symmetry and is localized principally on the phz component of the dppz ligand for all of the complexes. It is clear from these calculations that the relative energy of the LUMO decreases dramatically with the increasing electron withdrawing ability of the substituent located on a phz part of the ligand. TDDFT calculations for the lowest energy triplet excited states for gas-phase geometry-optimized *fac*-[ReCl(CO)$_3$(dppz-X$_2$)], with respect to the ground state, performed in a dielectric medium of 37.5 also show that the lowest triplet excited state for all complexes is MLCT (phz) and its energy decreases from **1** to **5**. However, the calculated transition energies could be underestimated because of the use of the BP functional and care must be taken when interpreting the relative energies of the excited states by this TDDFT method.

Although spectroelectrochemical and DFT studies have suggested that the LUMO in **1**−**5** is of phz nature, we are aware that for dppz complexes the photophysically active state is not always the lowest lying state. Thus, we cannot predict the nature of the photophysically active excited states from electrochemical measurements or from DFT calculations. Therefore we probed the photophysics of **1**−**5** directly with TRIR and emission spectroscopy. The use of TRIR is a particularly powerful tool, since (i) it allows observation of nonemissive excited states and (ii) the characteristic ν(CO) band shifts allow to unequivocally identify ^{3}IL(π-π*), ^{3}MLCT (phen), and ^{3}MLCT (phz) excited states.[12,33]

The TRIR spectra of **1**−**5** in CH$_2$Cl$_2$ obtained 100 ps following excitation (400 nm) are shown in Figure 5. All spectra show the depletion of the parent bands and production of new positive IR transient absorption bands. To clearly identify the nature of the excited state(s) formed following excitation we have primarily analyzed the high-frequency spectral window, 2000−2100 cm^{-1}.[34]

(32) The geometry-optimized ground-state structures for *fac*-[Re(Cl)(CO)$_3$(dppz-X$_2$)] (X = CH$_3$, F and Cl) calculated in the gas phase were compared with experimental structures, obtained from the X-ray diffraction. Calculated structures show good agreement with experimental data.

(33) (a) Turner, J. J.; George, M. W.; Johnson, F. P. A.; Westwell, J. R. *Coord. Chem. Rev.* **1993**, *125*, 101. (b) George, M. W.; Turner, J. J. *Coord. Chem. Rev.* **1998**, *217*, 217. (c) Vlček, A.; Farrell, I. R.; Liard, D. J.; Matousek, P.; Towrie, M.; Parker, A. W.; Grills, D. C.; George, M. W. *J. Chem. Soc., Dalton. Trans.* **2002**, 701. (d) Butler, J. M.; George, M. W.; Schoonover, J. R.; Dattelbaum, D. M.; Meyer, T. J. *Coord. Chem. Rev.* **2007**, *251*, 492.

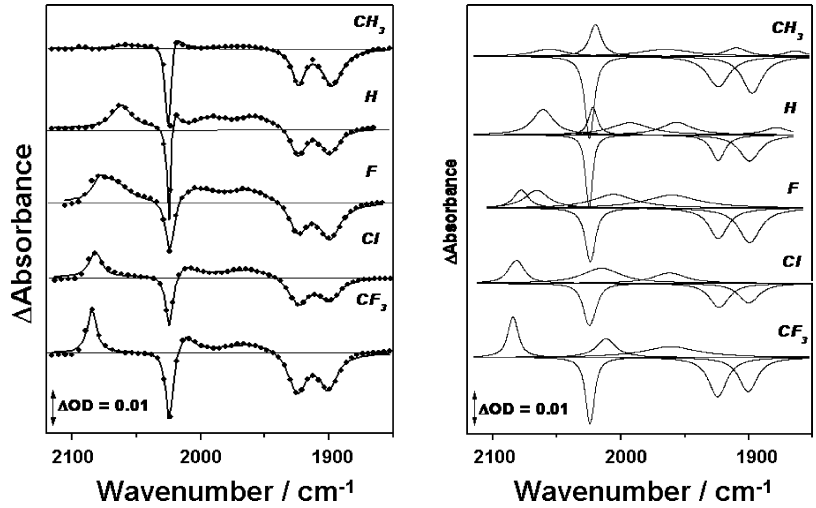

Figure 5. (a) TRIR spectra of *fac*-[ReCl(CO)$_3$(dppz-X$_2$)] obtained 100 ps following 400 nm excitation of CH_2Cl_2 solutions at room temperature (•) with the multicurve Lorentzian fit (line) and (b) the corresponding individual Lorentzian bands used to fit experimental spectra.

The TRIR spectra of **1**[35] and **2** show the two sets of transient bands, one of which is shifted to higher energy relative to the parent absorptions, characteristic of the ^{3}MLCT excited state.[33] The other set of transient bands shows a small negative shift relative to the parent bands and is assigned to a ^{3}IL(π-π*) excited state.[33] Further information can be obtained from analyzing the magnitude of the positive ν(CO) band shift accompanying the formation of the ^{3}MLCT state.[12] For **1** and **2** the magnitude of the positive ν(CO) band shift is about 40 cm^{-1}, which is typical of the ^{3}MLCT states of *fac*-[ReCl(CO)$_3$(α-diimine)] (α-diimine = 2,2′-bpy, phen)[33] and suggests the formation of a MLCT (phen) state for **1** and **2**. This conclusion is further confirmed by comparison with the available literature data for Redppz complexes, for example, 40 cm^{-1} shift is similar to the shift observed for *fac*-[Re(CO)$_3$(dppz-X$_2$)(4-Me$_2$Npy)]$^+$ (4-Me$_2$N-py = 4-(dimethyl)aminopyridine; X$_2$ = Cl$_2$,[12a] ^{1}/$_2$ COOEt,[12b] ^{1}/$_2$ NO$_2$[36]) which was assigned to a phen-localized ^{3}MLCT state. At the same time, the 40 cm^{-1} ν(CO) band shift is significantly smaller than the shift which was observed[10h,i,12] upon formation of MLCT (phz) excited state for *fac*-[Re(CO)$_3$(dppz)(py)]$^+$, **4**, and *fac*-[ReCl(CO)$_3$(dppz-COOEt)]. This allows the assignment of MLCT species formed following excitation of **1** and **2** in CH_2Cl_2 to a MLCT (phen) state.

The spectra of **3**, **4**, and **5** show the presence of only MLCT excited-state transient ν(CO) bands. The spectra of **4** and **5** contain only one set of transient bands shifted up relative to the parent bands (Table 3, Figure 5). This shift is considerably larger than that observed for MLCT (phen) states of **1** and **2** (e.g., ca. +60 cm^{-1} for the high frequency ν(CO) band) and indicates the formation of a MLCT (phz) excited state. The high frequency spectral region of **3** contains two transient ν(CO) bands of equal intensity, displaying shifts of 54 and 40 cm^{-1} relative to the parent absorption (Table 3, Figure 5). We tentatively assign these two bands to be due to MLCT (phz) and MLCT (phen) states, respectively.[34]

It should be noted that the spectra shown in Figure 5 correspond to a relatively late time delay (100 ps) and the interconversion of different excited states can occur on a faster time scale, since UV/visible excitation should populate both the ^{1}MLCT (phen) and ^{1}IL(π-π*) states. This has been discussed in detail previously[10g,12] for similar compounds. Additionally, the initially produced vibrationally hot electronic excited states can relax (i.e., $\pi_n \rightarrow \pi_0$) on the time scale of <20 ps.[37] The latter process is manifested in the change of the ν(CO) band shape, as the bands narrow and shift to a higher wavenumber.

The early time transformation of the TRIR spectrum is illustrated further in Figure 6a for **2** in CH_2Cl_2. It is clear that following excitation the new transients that are formed immediately after the flash narrow and shift to higher wavenumber within about 10 ps. The positions of transient ν(CO) bands obtained from TRIR spectra at late time delays after the vibrational cooling process is finished (>20 ps) are summarized in Table 3 and indicate the formation of both ^{3}MLCT (phen) and a small amount of ^{3}IL(π-π*) excited states.

Changes in the nature of the solvent may affect the photophysics of Redppz complexes, as observed during the light switch effect for [Ru(α-*diimine*)$_2$(dppz)]$^{2+}$ (α-*diimine* = bpy, phen). We have investigated the effect of solvent polarity on the photophysics of **2** by changing the solvent from the relatively nonpolar CH_2Cl_2 (ε = 8) to the more polar C_3H_7CN (ε = 24), Figure 6b. Solvent polarity is likely to affect the energy of both phen- and phz-based MLCT states, leaving the energy of the ^{3}IL (π-π*) state largely unaffected. Analysis of the high-wavenumber window of the TRIR spectra (2000−2100 cm^{-1}) of **2** in C_3H_7CN reveals

(34) In the 1900−2000 cm^{-1} spectral region fitting of the spectra to more than one excited state was complicated. Therefore the minimum number of Lorentzian bands was employed and no attempt was made to distinguish between the MLCT (phen) and MLCT (phz) features.

(35) The low intensity of the MLCT bands of **1** made it difficult to fit the lower frequency bands in the 1900−2000 cm^{-1} region and one Lorentzian band for MLCT features was employed instead of two. Fitting using two Lorentzian bands for this MLCT feature did not produce a significantly better fit.

(36) Dyer, J.; Grills, D. C.; Matousek, P.; Parker, A. W.; Towrie, M.; Weinstein, J. A.; George, M. W. *Chem. Commun.* **2002**, 872.

(37) Dougherty, T. P.; Heilweil, E. J. J. *Chem. Phys.* **1994**, *100*, 4006.

Table 3. TRIR Data for *fac*-[ReCl(CO)$_3$(dppz-X$_2$)] in CH_2Cl_2, CH_3CN, and C_3H_7CN Obtained at 100 ps Time Delay Following 400 nm Excitation of These Solutions

compound	X	solvent	parent, ν(CO)/cm^{-1}	excited State, ν(CO)/cm^{-1}	lifetime/ns	nature of the excited state(s)
1	CH_3	CH_2Cl_2	1903, 1923, 2025	1864, 1910, 2020 1965[a], 2056	420 (±80)[b]	IL $\pi\pi^*$ MLCT (phen)
1	CH_3	CH_3CN	1902, 1919, 2024	1890, 1913, 2020 1960, 2005, 2066	4.7 (±0.5)	IL $\pi\pi^*$ MLCT (phen)
2	H	CH_2Cl_2	1900, 1921, 2024	1870, 2022 1956, 1993, 2061	40 (±10)	IL $\pi\pi^*$ MLCT (phen)
2	H	C_3H_7CN	1901, 1920, 2024	1890, 2018 1963, 2015, 2072[a] 2087	3.5 (±1.0)	IL $\pi\pi^*$ MLCT (phen) MLCT (phz)
2	H	CH_3CN	1901, 1920, 2024	1890, 2018 1963, 2015, 2073[a] 2087	2.5 (±0.8)	IL $\pi\pi^*$ MLCT (phen) MLCT (phz)
3	F	CH_2Cl_2	1900, 1921, 2024	1960[a], 2006[a], 2064 2078	3.05 (±0.04)	MLCT (phen) MLCT (phz)
3	F	C_3H_7CN	1900, 1917, 2024	1970, 2003, 2090	0.33 (±0.05)	MLCT (phz)
3	F	CH_3CN	1900, 1917, 2024	1970, 2003, 2091	0.24 (±0.02)	MLCT (phz)
4	Cl	CH_2Cl_2	1901, 1923, 2025	1960, 2013, 2082	1.5 (±0.2)	MLCT (phz)
4	Cl	CH_3CN	1902, 1920, 2024	1978, 2017, 2094	0.15 (±0.02)	MLCT (phz)
5	CF_3	CH_2Cl_2	1904, 1924, 2025	1961, 2012, 2084	0.30 (±0.02)	MLCT (phz)
5	CF_3	CH_3CN	1903, 1920, 2024	1974, 2010, 2093	0.043 (±0.005)	MLCT (phz)

[a] In the 1900−2000 cm^{-1} spectral region fitting to more than one excited state was complicated. Therefore the minimum number of Lorentzian bands was employed and no attempt was made to distinguish between MLCT (phen) and MLCT (phz) features. [b] The low signal/noise ratio did not permit the accurate determination of the excited-state lifetime.

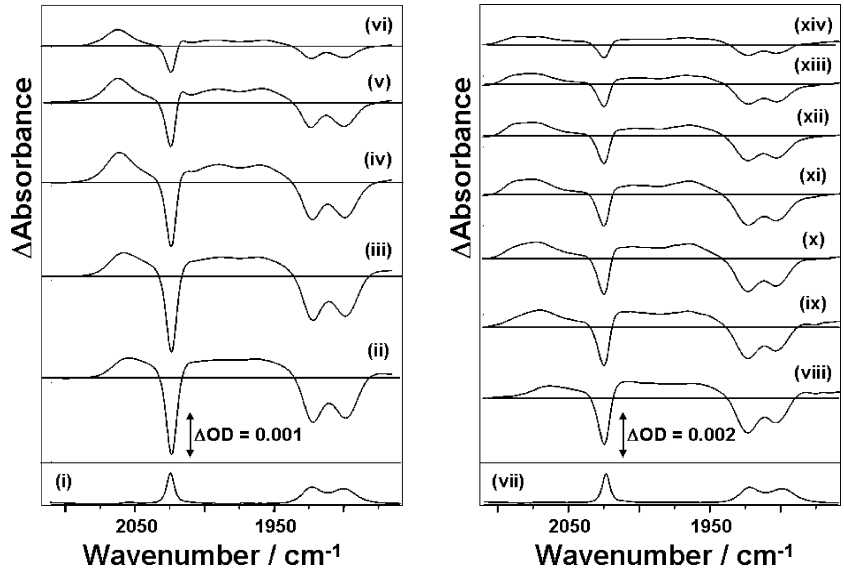

Figure 6. (i) FTIR spectra of *fac*-[ReCl(CO)$_3$(dppz)] in CH_2Cl_2 at room temperature. TRIR spectra of *fac*-[ReCl(CO)$_3$(dppz)] in CH_2Cl_2 obtained (ii) 2 ps; (iii) 4 ps; (iv) 20 ps; (v) 100 ps; and (vi) 2 ns after 400 nm excitation. (vii) FTIR spectra of *fac*-[ReCl(CO)$_3$(dppz)] in C_3H_7CN at room temperature. TRIR spectra of *fac*-[ReCl(CO)$_3$(dppz)] in C_3H_7CN obtained (viii) 2 ps; (ix) 10 ps; (x) 20 ps; (xi) 70 ps; (xii) 500 ps; (xiii) 1 ns; and (xiv) 2 ns after 400 nm excitation.

that at time delays >70 ps there are two distinct transient bands shifted to higher wavenumber centered at 2072 and 2087 cm^{-1}. For these two transient bands the shifts upon formation of the MLCT excited state are 48 and 63 cm^{-1}, and these bands are assigned to formation of phen- and phz-based MLCT states, respectively, which then decay to reform the ground state with the lifetime of 3.5 (±1.0) ns. The transient bands narrow and shift slightly to higher wavenumber within the first few picoseconds, consistent with the cooling process of the initially formed vibrational excited states. However, the TRIR spectrum continues to change between 20 and 70 ps and it is clear that vibrational cooling alone can not account for these slower processes. Thus, we assign these changes to a partial decay (time constant of ca. 25 ps) of the initially formed MLCT (phen) excited state of **2** to a relaxed equilibrium of MLCT (phen) and MLCT (phz) excited states. The TRIR spectra of **2** in C_3H_7CN also reveal that excitation produces a small amount of the ^{3}IL(π-π^*) state, but we were unable to monitor dynamics of this species.

The TRIR spectra observed for **2** in CH_3CN (ε = 36.5) are similar to those measured in C_3H_7CN, Table 3. The MLCT (phen) excited state of **2** in CH_3CN partially decays (time constant of ca. 10 ps) to a relaxed equilibrium of MLCT (phen) and MLCT (phz) excited states.[38] The excited states of **2** decay to the ground state with a lifetime of 2.5 (±0.8) ns, which is faster than the decay observed in C_3H_7CN. Thus,

(38) Both vibrational cooling and MLCT (phen) to MLCT (phz) conversion contribute to the observed TRIR signal at early times.

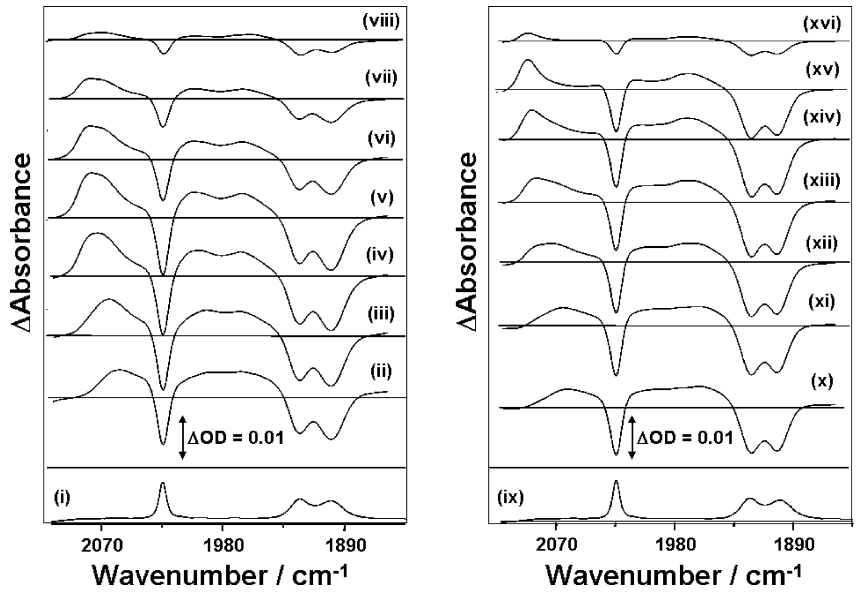

Figure 7. (i) FTIR spectra of *fac*-[ReCl(CO)$_3$(dppz-F$_2$)] in CH_2Cl_2 at room temperature. TRIR spectra of *fac*-[ReCl(CO)$_3$(dppz-F$_2$)] in CH_2Cl_2 obtained (ii) 2 ps; (iii) 4 ps; (iv) 20 ps; (v) 500 ps; (vi) 1 ns; (vii) 2 ns; and (viii) 4 ns after 400 nm excitation. (ix) FTIR spectra of *fac*-[ReCl(CO)$_3$(dppz-F$_2$)] in C_3H_7CN at room temperature. TRIR spectra of *fac*-[ReCl(CO)$_3$(dppz-F$_2$)] in C_3H_7CN obtained (x) 1.5 ps; (xi) 2 ps; (xii) 4 ps; (xiii) 6 ps; (xiv) 10 ps; (xv) 100 ps; and (xvi) 500 ps after 400 nm excitation.

it is clear that raising the polarity of the solvent has a dramatic effect by increasing the final population and the rate of formation of MLCT (phz). We have explored this further by examining the photophysics of the other complexes in more polar solvents.

The parent and transient band positions and excited-state lifetimes, obtained for **2, 3** in C_3H_7CN and for **1**−**5** in CH_3CN and CH_2Cl_2 are summarized in Table 3. It is clear that the excited-state lifetimes for all complexes studied are shortened in solutions of increased polarity. We also note that the shift in ν(CO) upon formation of the MLCT (phz) excited state is larger in the more polar CH_3CN compared to CH_2Cl_2.

The change in the rate of MLCT (phz) formation upon an increase in the polarity of the solvent can be further demonstrated by monitoring the early time dynamics in the TRIR spectra of **3** in CH_2Cl_2 and C_3H_7CN, Figure 7. It is clear that for **3** in C_3H_7CN at time delays >10 ps only IR bands attributed to the MLCT (phz) excited state are observed. In stark contrast, the excited spectra of **3** recorded in CH_2Cl_2 show the presence of an equilibrated mixture of approximately equal amounts of both MLCT (phen) and MLCT (phz) excited states at times from 2 ps to 10 ns. Therefore, the TRIR data for **2** and **3** clearly demonstrate that in both CH_3CN and C_3H_7CN there is a higher population of a MLCT (phz) state in comparison to less polar CH_2Cl_2. These results are consistent with the lowering of MLCT (phz) excited-state energy with increasing polarity. Charge separated excited states are more stabilized in solvents with higher polarity, for example, the ^{3}MLCT state of $[Ru(bpy)_3]^{2+}$.[20] Our present data indicate that the MLCT (phz) state is stabilized more than that of MLCT (phen) in more polar solvents, possibly because of the higher degree of charge separation in the former.

Hydrogen bonding has been suggested to be one of the major factors determining the light switch behavior of $[Ru^{II}(\alpha\text{-}diimine)_2(dppz)]^{2+}$. We have investigated the effect of hydrogen bonding solvents by repeating the TRIR measurements of **3** in C_3H_7OH and CH_3OH.[39] The TRIR spectra obtained for **3** in these solvents are similar to those obtained in C_3H_7CN, Table 3. However, the dynamic behavior, that is, the rate of interconversion between MLCT (phen) and MLCT (phz) states, is different, Figure 8. The data can be fitted to a biexponential function, giving the lifetimes of 51 (±6) and 250 (±40) ps (C_3H_7OH) and 9 (±2) and 90 (±10) ps (CH_3OH) for the conversion of MLCT (phen) to MLCT (phz) states and subsequent decay of MLCT (phz), respectively. Table 4 summarizes all the lifetimes for the conversion of MLCT (phen) → MLCT (phz) states and excited-state decay for **3** in all solvents. We can directly examine the effect of H-bonding on the photophysics of **3** by comparing the excited-state lifetimes of **3** in the solvents of similar polarity, C_3H_7CN/C_3H_7OH and CH_3CN/CH_3OH. This comparison indicates that increasing both polarity and H-bonding ability of the solvent shorten the MLCT (phz) excited-state lifetime and alter the dynamics of its formation. These direct observations confirm that both solvent polarity and hydrogen bonding contribute to the mechanism of the light switch effect.

TRIR studies of **1**−**5** have clearly shown that MLCT (phz), MLCT (phen), and ^{3}IL(π-π*) states play an important role in the photophysics of these complexes. By directly monitoring the population of these states, we have determined that it is affected by the nature of substituents on the dppz ligand,

(39) We were unable to perform TRIR studies on **1**, **2**, **4** in hydrogen bonding solvents because of their low solubility and short pathlength required for these IR experiments. The TRIR spectrum of **5** in CH_3OH was assigned to MLCT (phz) excited state with excited state lifetime of ca 30 ps.

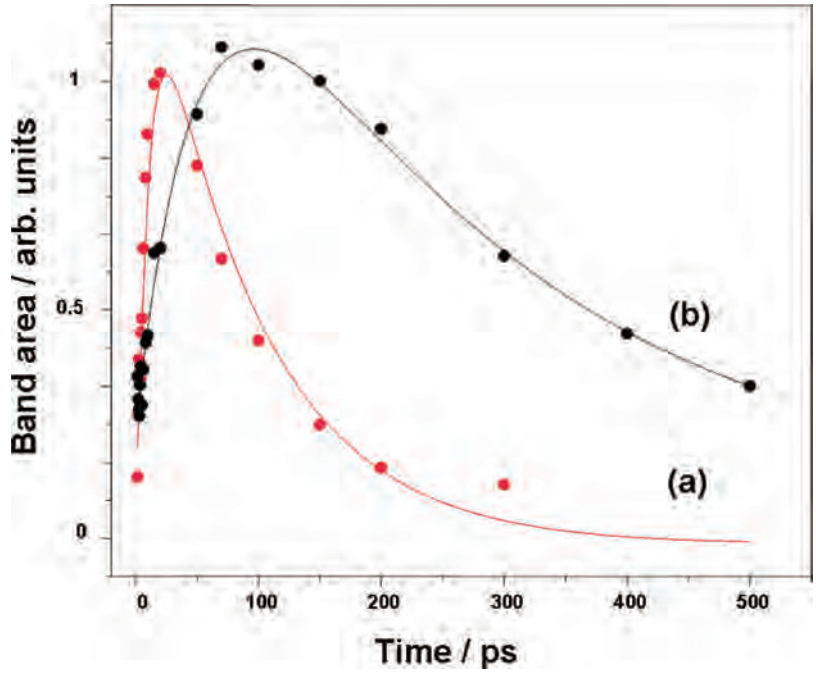

Figure 8. Kinetic traces obtained from the multicurve Lorentzian fit of the high frequency ν(CO) MLCT bands of TRIR spectra for *fac*-[ReCl(CO)$_3$(dppz-F$_2$)] in (a) CH_3OH (red line) and (b) C_3H_7OH (black line) following 400 nm excitation. Solid lines are biexponential fits for the data, $\tau = 9$ ($\pm$2) ps and 90 ($\pm$12) ps (CH_3OH) and $\tau = 51$ ($\pm$6) ps and 250 ($\pm$40) ps (C_3H_7OH).

Table 4. Excited State Lifetime and Characteristic Time of MLCT (phen) to MLCT (phz) Conversion Obtained with *ps*-TRIR for *fac*-[ReCl(CO)$_3$(dppz-F$_2$)] in Different Solvents Following 400 nm Excitation of These Solutions[c]

solvent	ε	α[a]	lifetime$_{\text{MLCT (phen)}\rightarrow\text{ MLCT (phz)}}$/ps	lifetime$_{\text{MLCT (phz)}}$/ps
CH_2Cl_2	8	0.22	ca. 6[b]	3050 ($\pm$40)
C_3H_7OH	20	<0.86[b]	51 ($\pm$6)	250 ($\pm$40)
C_3H_7CN	24	<0.15[d]	6 ($\pm$0.2)	330 ($\pm$5)
CH_3OH	35	0.98	9 ($\pm$2)	90 ($\pm$12)
CH_3CN	36.5	0.15	4 ($\pm$0.5)	240 ($\pm$20)

[a] The parameter α characterizes the hydrogen bonding ability of the solvent, from ref 12. [b] Both MLCT (phen) and MLCT (phz) states are present at late time delays and decay in equilibrium, which complicates the fitting of the spectra to obtain kinetic traces for MLCT (phen)$\rightarrow$ MLCT (phz) conversion. [c] Less than the value for C_2H_5OH. [d] Less than the value for CH_3CN.

the polarity, and the hydrogen bonding ability of the solvent. We were also able to directly monitor the solvent-dependent interconversion of MLCT (phen) and MLCT (phz) excited states, implied in the mechanism of the light switch effect of [Ru(α-diimine)$_2$(dppz)]$^{2+}$. Our data agree with the conclusions of the emission study[6,7] that the higher lying MLCT (phen) state is preferentially populated over the energetically lowest MLCT (phz).

To correlate our TRIR observations with the variable temperature emission study of [Ru(α-diimine)$_2$(dppz)]$^{2+}$, we have examined the emission properties of **1**$-$**5** in CH_2Cl_2 and CH_3CN. In CH_3CN solution at room temperature, we can only detect luminescence from **1** and **2** which is assigned to emission from MLCT excited states consistent with TRIR studies. It is possible that an equilibrium between the MLCT (phen) excited state and a close lying ^{3}IL(π-π*) state exists as both states were observed in the ps-TRIR experiment. Indeed, earlier time-resolved resonance Raman studies indicate that for **2** ^{3}IL(π-π*) is the lowest in energy in CH_3CN, even though it is a MLCT emitter.[40] On the basis of the TRIR data we can assign the emission to the phen-based MLCT excited state.

We did not detect any emission from **3** in CH_3CN at room temperature consistent with the short lifetime ($\tau = 240$ ps) of the MLCT (phz) excited state. However this complex shows a weak emission band in CH_2Cl_2 solution at room temperature centered at about 650 nm (Figure 9a) with a lifetime ($\tau = 2.8$ ($\pm$0.1) ns) consistent with the decay of the excited-state bands observed in the TRIR experiments. The observation of emission following the excitation of **3** in CH_2Cl_2 is consistent with ps-TRIR data for this complex, showing the mixture of MLCT (phen) and MLCT (phz) states. We have recorded the emission spectra of **3** in CH_2Cl_2 as a function of temperature over the range of 190 to 300 K, Figure 9b. The emission decreases as the temperature is lowered and this unusual temperature dependence is consistent with the presence of a low-lying MLCT (phz) state, characterized by fast nonradiative decay, which we have directly observed with TRIR. We can compare these observations for **3** with emission studies reported for the light-switch mechanism of [Ru(α-diimine)$_2$(dppz)]$^{2+}$ where a similar decrease of emission in CH_3CN with decreasing

(40) Schoonover, J. R.; Bates, W. D.; Meyer, T. J. *Inorg. Chem.* **1995**, *34*, 6421.
(41) Gerson, F.; Huber, W. *Electron Spin Resonance Spectroscopy of Organic Radicals*; Wiley-VCH: Weinheim, 2003.

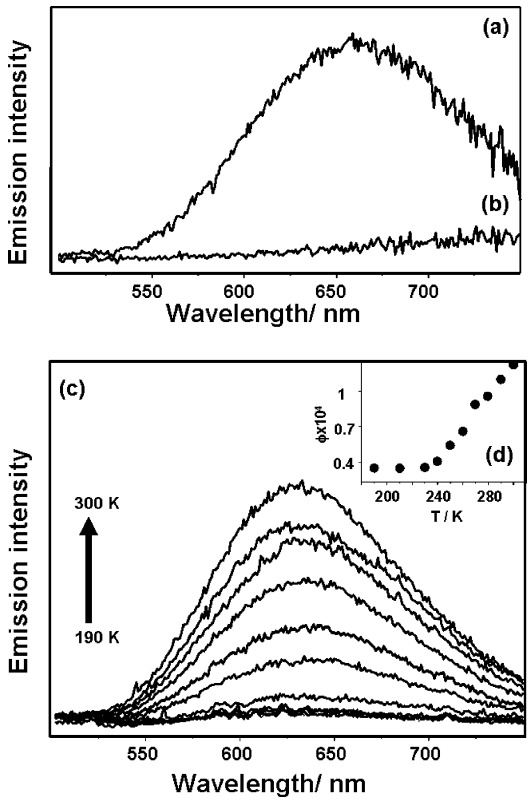

Figure 9. Corrected emission spectra of *fac*-[ReCl(CO)$_3$(dppz-F$_2$)] in (a) CH_2Cl_2 and (b) CH_3CN obtained with 360 nm excitation; (c) series of emission spectra obtained for *fac*-[ReCl(CO)$_3$(dppz-F$_2$)] in CH_2Cl_2 in the temperature range from 190 to 300 K; (d) the inset shows the temperature dependence of emission quantum yield for this complex.

temperature was observed.[6a] The results on [Ru(α-diimine)$_2$(dppz)]$^{2+}$ were interpreted as entropy-governed population of the "dark" MLCT (phz) state. We cannot rule out the possibility of a weak emission from the MLCT (phz) state, as pure MLCT (phz) states in **4** and **5** in CH_3CN are too short-lived (as indicated by TRIR) to observe such emission. However, the TRIR results show that the MLCT (phz) state of **4** in CH_2Cl_2 decays with a lifetime of 1.5 ns and gives us the opportunity to directly monitor the emission of a pure MLCT (phz) state. We do observe a very weak emission centered at 720 nm with a lifetime of 1.5 ns which we tentatively assign to emission from the MLCT (phz) state of **4** in CH_2Cl_2.

Conclusions

We have used a combination of (spectro)electrochemical, emission, and TRIR measurements to probe the nature of the frontier orbitals and the resulting excited state in the series of *fac*-[ReCl(CO)$_3$(dppz-X$_2$)] (X = CH_3, H, F, Cl, CF_3) (**1**−**5**). For all complexes the LUMO is a phenazine based orbital localized on the dppz ligand. We observe that three different excited states, IL $\pi\pi^*$, MLCT (phen), and MLCT (phz) are formed depending upon the substituents on the dppz ligand and on the nature of the solvent. We find that the MLCT (phz) state possesses a low emission quantum yield and is not always significantly populated, consistent with previous reports for other dppz containing complexes.[6,7] We were able to tune the energy of the MLCT (phz) state by increasing the acceptor ability of the substituent X. For the complexes which did not contain strong electron withdrawing substituents X, **1**−**3**, the population of the MLCT (phen) and IL $\pi\pi^*$ states was observed experimentally with TRIR and emission from the MLCT (phen) state was demonstrated. Our experimental observations were confirmed by DFT calculations.

Our results for **1**−**5** are directly related to the light switch effect,[4–7] well documented for complexes such as [Ru(bpy)$_2$(dppz)]$^{2+}$, since there is an increase or decrease in emission with the change in environment for the series of **1**−**5**. The present findings for **1**−**5** in nonaqueous solvents can be rationalized on the basis of the competition between energetic factors acting in favor of the dark MLCT (phz) state and entropic factors, favoring an emissive MLCT (phen) state. We were able to tune the relative population of these two states within one molecule by controlling the polarity of the environment, the hydrogen bonding ability of the solvent, and temperature. This approach opens up the possibility to finely tune the energy (and therefore population) of both MLCT (phz) and MLCT (phen) states either by introducing substituents with different donor/acceptor ability or altering the environment of the chromophore. This wealth of excited-state properties and understanding of their intricate interplay can be utilized to create switches and probes based on Re dppz transition metal complexes to detect changes in complex environments such as those found within DNA double helices or intracellular matrices, following the development of the intracellular delivery strategies for such complexes.[42]

Acknowledgment. We would like to acknowledge Dr Ian P. Clark for assistance with emission measurements performed with the CCD camera. We thank the EPSRC, ORS (M.K.K.) and The University of Nottingham for financial support. We thank STFC for funding access to the Central Laser Facility to perform the time-resolved IR studies. We acknowledge the EPSRC National Crystallography Service at the University of Southampton for the collection of X-ray diffraction data on compound **3**.

Supporting Information Available: Geometrical parameters obtained from experiments and calculations, and the energies and composition for the DFT-calculated frontier orbitals. This material is available free of charge via the Internet at http://pubs.acs.org.

IC800753F

(42) Amoroso, A. J.; Coogan, M. P.; Dunne, J. E.; Fernandez-Moreira, V.; Hess, J. B.; Hayes, A. J.; Lloyd, D.; Millet, C.; Pope, S. J. A.; Williams, C. *Chem. Commun.* **2007**, 3066–3068.